The Right Direction to Smell: Efficient Sensor Planning Strategies for Robot Assisted Gas Tomography

Muhammad Asif Arain*, Erik Schaffernicht, Victor Hernandez Bennetts and Achim J. Lilienthal

***Abstract*— Creating an accurate model of gas emissions is an important task in monitoring and surveillance applications. A promising solution for a range of real-world applications are gas-sensitive mobile robots with spectroscopy-based remote sensors that are used to create a tomographic reconstruction of the gas distribution. The quality of these reconstructions depends crucially on the chosen sensing geometry. In this paper we address the problem of sensor planning by investigating sensing geometries that minimize reconstruction errors, and then formulate an optimization algorithm that chooses sensing configurations accordingly. The algorithm decouples sensor planning for single high concentration regions (hotspots) and subsequently fuses the individual solutions to a global solution consisting of sensing poses and the shortest path between them. The proposed algorithm compares favorably to a template matching technique in a simple simulation and in a real-world experiment. In the latter, we also compare the proposed sensor planning strategy to the sensing strategy of a human expert and find indications that the quality of the reconstructed map is higher with the proposed algorithm.**

I. Introduction

Fugitive gas emissions are a major concern in many industrial settings due to their impact on safety, environment and economics. The first step in monitoring applications is the detection of gas leaks in the environment, a problem we addressed in our previous work [1], [2]. After gas sources have been detected, the next step is to investigate the exact location and magnitude of the leakage, by building a gas distribution map. The whole process is visualized in Fig. 1.

Robot assisted gas tomography (RAGT), inspired by computer tomography of gases (CTG), has been introduced recently as a new method to build gas distribution maps with robots using remote gas sensors [3]. Unlike CTG, which collects data using a set of remote sensors placed at fixed locations, RAGT combines mobile robots with remote sensors (Fig. 2(a)) to take advantage of the robot's mobility and thus allows for flexible sensor placements. The gas sensor we are using is a tunable diode laser absorption spectroscopy (TDLAS) sensor. These sensors are highly selective and sensitive for their target gas, long-term stable, and they report integral concentration measurements along the line-of-sight over distances up to 30 m. However, they return spatially unresolved measurements, which do not show the distribution of gas along the measurement path (Fig. 2(b)).

The authors are with Mobile Robotics & Olfaction (MRO) Lab, Center of Applied Autonomous Sensor Systems (AASS), Örebro University, SE-70182 Örebro, Sweden.

*Corresponding author <asif.arain@oru.se>

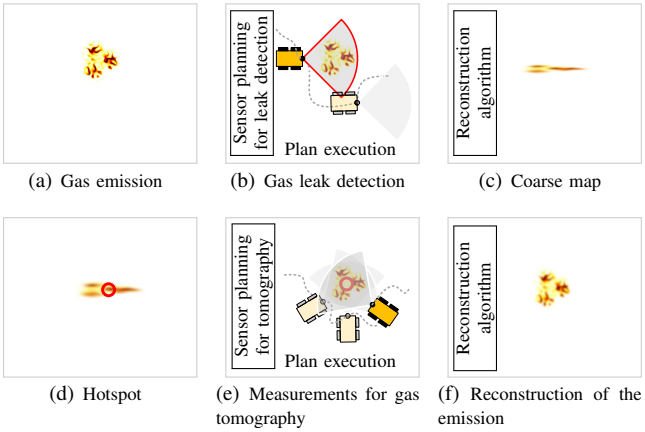

(a) Gas emission (b) Gas leak detection (c) Coarse map

(d) Hotspot (e) Measurements for gas tomography (f) Reconstruction of the emission

Fig. 1. Emission monitoring scenario with a mobile robot considered in this paper. Gas emission (a) is detected executing the *sensor planning algorithm for gas detection*, see [2] (b). A coarse gas distribution map is generated with the robot assisted gas tomography algorithm, see [3] (c), and a hotspot is identified in the coarse map (d). Next, a sensing geometry is planned using the *sensor planning algorithm for tomography*, which is the contribution of this paper (e). Finally, we obtain a high quality reconstruction using again the robot assisted gas tomography algorithm in [3] (f).

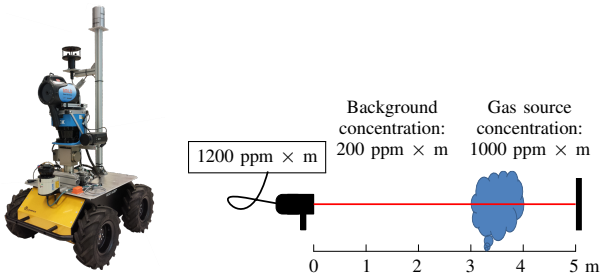

(a) (b)

Fig. 2. (a) Gasbot robot is equipped with an actuated TDLAS sensor. (b) TDLAS sensor reports integral concentration of methane along its line-of-sight (ppm × m).

For a RAGT reconstruction, the area of interest has to be observed from different viewpoints. The number of measurement locations and the sensor pose is commonly referred to as the sensing geometry. In CTG, the problem of determining an effective sensing geometry has been previously addressed in [4]–[8]. However, the results can not be directly applied to RAGT in general and the sensing system we use in particular due to, (1) the evaluation is presented for the different sensing technologies such as differential optical absorption spectroscopy (DOAS) and open-path Fourier transform infrared (OP-FTIR) spectrometers that include fixed mirrors and reflectors resulting in complex optical paths, (2) options of sensor placements are limited, whereas a robot

can perform sensing actions at many different positions. The problem of selecting a proper sensing geometry has not been addressed in the context of robotics yet, previous work [3] used predefined sensing positions selected by a human expert. We will discuss the specifics in Sec. II.

Another aspect of a successful measurement strategy is the minimization of the time required to take all the measurements to build a good map. Minimizing exploration time in mobile robot olfaction has been explored for gas detection coverage problems in our previous work [2] and by Atanasov *et.al.* [9] who proposed an expectation maximization framework. We are not aware of any previous work that takes into account sensing geometries. The main contribution of this work is an optimization algorithm addressing sensor planning for RAGT considering sensing geometries, which we describe in Section III.

Section IV describes another important contribution: the comparison of the proposed algorithm against a heuristic solution and the strategy of a human expert in simulation and a real-world scenario using the Gasbot robotic platform [10].

II. Sensing Geometries

We consider a robot equipped with an actuated remote gas sensor that performs the following basic sensing action (Fig. 3): at pose p, the robot scans a circular sector of radius r and angle ϕ by carrying out a sequence of s line measurements. A sensing configuration $c_i = (p_i, \phi_i, r_i)$ is thus a sensing action with parameters ϕ_i and r_i, performed by the robot at pose p_i. The set of sensing configurations performed by a robot at a given area is called the sensing geometry.

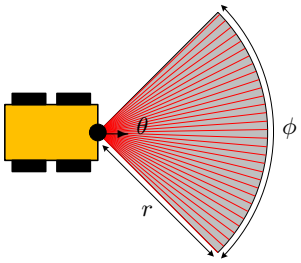

Fig. 3. A sensing action is the sampling of a circular sector (ϕ, r) by emitting s optical beams.

As previously stated, sensing geometries are crucial to estimate the spatial distribution of the gas concentrations. We thus carried out an evaluation of different sensing geometries using an ad-hoc simulation environment, which models the gas distribution as a summation of spatially distributed Gaussian plumes of different concentration. Examples of the gas distributions used are shown in Fig. 4.

To evaluate the effect of the geometries, a set of n_c sensing configurations are placed in concentric circles around the area of interest. Tomographic reconstruction is carried out using the least squares approach presented in [11]. As a metric for the reconstruction quality, the mean squared error (MSE) between the reconstruction and the initial concentration was computed.

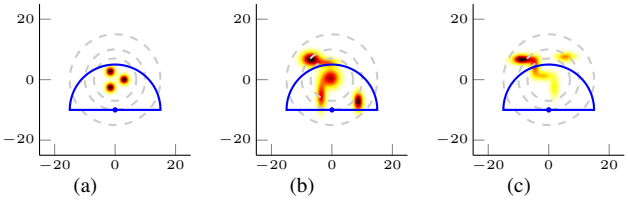

Fig. 4. Simulated 50 × 50 m^2 environment models. Dark colors represent higher concentrations; the gray dotted lines show circles of 7 m, 10 m and 15 m radius where sensing configurations were distributed. One example configuration, in blue, is placed at the circle of 10 m. (a) shows the model where high concentration region is located at the center, and (b)-(c) show the models where the investigated gas dispersion pattern are uneven.

In the simulation, geometries of $n_c = [2, 3, 4]$ configurations are placed at different positions, always facing the center of the area of interest. In the case of $n_c = 2$, the angular displacement between the configurations is incrementally changed 10° counter clockwise for a total of 35 different geometries. For $n_c = 3$, the configurations are placed with pair-wise angular displacements of a counter clockwise incremental step of 10°, for a total of 1190 geometries. For $n_c = 4$ the first three configurations corresponding to the best reconstruction of $n_c = 3$ are fixed. The fourth configuration is then placed at incremental steps of 10°. Therefore, a total of 33 reconstructions are computed. All the geometries were evaluated using the combination of parameters $\phi = [90°, 180°]$, $r = 15$ m and $\Delta s = 1°$. Furthermore, each configuration was investigated with different distances (5 m, 7 m and 15 m) from the area of interest.

We used four environment models: two of them with high concentration regions located only at the center of the map, and two with uneven gas dispersion patterns. The models with the area of interest at the center can be fully covered with the configurations placed at 7 m and 10 m distances, while the configurations placed at the distance 15 m might miss parts of the actual gas concentration. This scheme helps to investigate how the cross angles effect the reconstruction quality when the configurations are placed at different distances.

The evaluation, which is partially shown in Fig. 5 suggests that, for $n_c = 2$ the best reconstruction quality is obtained when the pairwise angular displacement between sensing configurations is equal to 90° (Fig. 5(a)). For $n_c = 3$, the reconstruction quality is further improved using a pairwise angular displacement of 60° or 120° (Fig. 5(b)). Adding a fourth configuration does not show a significant improvement in the reconstruction quality. Therefore, we conclude that for the reconstruction of a high concentration region $n_c = 3$ with pairwise angular displacement of 60° or 120° is a good choice to maximize the reconstruction quality. We will approximate the (flipped) functions shown in Fig. 5 with Gaussians (see Eq. 3) and use this function G to express the expected reconstruction quality (ERQ) for a given set of sensing configurations.

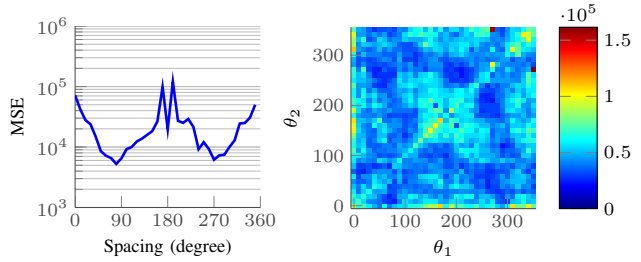

(a) $n_c = 2$ (b) $n_c = 3$

Fig. 5. (a) The mean squared error (MSE) between the ground truth and its reconstruction is shown for the set of 2 configurations ($n_c = 2$). On the x-axis is the angular displacement between the configurations and on the y-axis is the MSE. The least reconstruction error and therefore highest reconstruction quality can be observed for cross angles of 90°. (b) The MSE is shown in the color code on the right for the set of 3 configurations ($n_c = 3$). Along x-axis is the pair-wise angular displacement between the configurations 1 and 2 (θ_1), and along y-axis is the pair-wise angular displacement between the configurations 1 and 3 (θ_2). The results suggest that the reconstruction quality is best when pair-wise cross angles are 60° and 120° on a half circle.

III. Sensor Planning

The total exploration time is the sum of the sensing time, and the traveling time between sensing configurations. We define the problem on a Cartesian grid map with discrete candidate sensing configurations. A valid solution is an ordered list of k sensing configurations, with its cost expressed as:

$$cost(\pi) = \sum_{i=1}^{k-1} t^m_{p_i \to p_{i+1}} + t^m_{p_k \to p_1} + \sum_{c_i \in \pi} t^s_{c_i} \qquad (1)$$

where $t^m_{p_i \to p_{i+1}}$ is the time for the movement from pose p_i to p_{i+1}, $t^m_{p_k \to p_1}$ to close the loop and $t^s_{c_i}$ is the sensing time of configuration c_i.

Given the set Π of all valid solutions to a given problem instance, then optimal solution π_{opt} is the one with minimum cost and an ERQ above a chosen threshold[1] $\mathfrak{n}$:

$$\pi_{opt} = \underset{\pi_i \in \Pi}{\operatorname{argmin}}\, cost(\pi_i) \;\text{ s.t. }\; \text{ERQ} \geq \mathfrak{n} \qquad (2)$$

Estimating the ERQ for arbitrary large problems is not possible due to the size of the search space. Therefore, we split the overall problem into local subproblems (hotspots) where we can use the results of the previous section to estimate the ERQ.

A. The xvt-SPP Algorithm

The overall procedure of our approach is shown in Algorithm 1.

The identification of high concentration regions on a map can be performed either by a human expert or as a result of a gas detection tour using the algorithm in [1], [2]. In the latter case, we build a preliminary tomographic reconstruction, which is very inaccurate due to sensing geometries that have almost no overlapping field of views. A hotspot is defined by the mean position of cells with a concentration above a threshold within neighborhood d (1.5 m in our implementation).

[1]We are avoiding the formulation of a multi-criteria optimization problem here by not maximizing the expected reconstruction quality, but considering it as a constraint instead.

Algorithm 1 xvt-SPP

1: Identify high concentration regions (hotspots);
2: Solve TSP for the hotspots (and start position) to approximately determine entry and exit directions of the robot for each hotspot;
3: For each hotspot, find a sensing geometry with maximum ERQ (Eq. 5) taking into account entry and exit direction;
4: Combine the local sensing configurations by removing overlapping redundant configurations (Eq. 7);
5: Solve TSP for the configurations and the start position to find a tour;
6: Execute tour and apply the tomographic reconstruction algorithm [11] to build GDM;
7: OPTIONAL: Identify high concentration region(s) and go back to step 2 to refine the GDM;

We introduce global information into the local subproblems by determining approximate entry and exit directions of the robot for each subproblem by solving a traveling salesman problem (TSP) between all hotspots and the robot's starting position.

B. Local Solutions

Each hotspot is considered as an individual problem of reconstruction. For a single high concentration region, pair-wise cross angles between the beams from different sensing positions can be defined in a square matrix A of the number of candidate sensing configurations. The ERQ G for the cross angles can be approximated with the two overlapping Gaussian functions of mean 60° and 120° as:

$$G_{n_c=3} = \sum_{\forall \mu \in M} 0.5 e^{\frac{-(A-\mu)^2}{2\sigma^2}}, \quad \sigma = 10°, M = \{60°, 120°\} \qquad (3)$$

This function integrates the results from the investigation of different sensing geometries from Sec II into the optimization process.

While the center of the hotspot is used to define the focus point for the choice of cross angles, it is required that we also cover all other local cells that reported gas concentration above the threshold during the gas detection step. This sensing coverage of the hotspot for the candidate configurations is defined by a discrete visibility matrix:

$$V[a, c] = \begin{cases} 1 & \text{if } a \in v_{\mathcal{P}}(c) \\ 0 & \text{otherwise} \end{cases} \qquad (4)$$

where $v_{\mathcal{P}}(c)$ is a function that generates a list of the cells visible from configuration c. This concept of sensing coverage was already used for the sensor planning for gas detection, hence a more detailed explanation for this part is available in [1].

The candidate sensing configurations C around each hotspots are defined on the movement graph within the sensing range that can cover the hotspot. For the vector C of candidate configurations, the ERQ for the cross angles is $C'GC$ and the sensing coverage is VC.

The distance vector D encodes the travel time from the reference point to each sensing configuration. This reference point is used to include information from the global problem and is chosen as mean of entry and exit direction with a distance of half the sensing range $r/2$ from the hotspot, see Fig. 6.

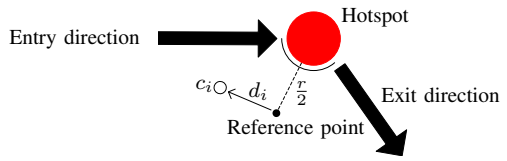

Fig. 6. Example for the reference point system. Sensing configurations close to this point are preferred.

The problem is then formalized as an optimization problem in Eq. 5. The objective function (Eq. 5a) integrates the terms discussed above. Eq. 6 represents the goals of covering the hotspot thoroughly and minimizing the time to do so. The parameter β between 0 and 1 (we use $\beta = 0.5$) is the trade-off between those two goals. The first part of Eq. 5a represents the goal of having an optimal sensing geometry according to Section II and is balanced against the exploration time minimization by the parameter α (we use $\alpha = 0.75$). Higher values of α correspond to a solution with a better ERQ of cross angles that will be preferred instead of the combination of sensing coverage and the traveling distance. Similarly, between sensing coverage and the traveling distance, higher β will influence the solution towards the complete coverage of the positive concentration cells. The constraint in Eq. 5b limits the number of selected configurations to n.

$$\underset{C}{\text{maximize}} \quad \alpha C'GC + (1-\alpha)C'U \tag{5a}$$

subject to

$$\mathbf{1}'C \leq n \tag{5b}$$

$$C \in \{0,1\} \tag{5c}$$

$$U = \beta(\overline{\mathbf{1}'V}) + (1-\beta)(1-\overline{D})) \tag{6}$$

Since, solving the optimization problem in Eq. 5 with high number of variables is computational demanding, we considered a limited number of variables (200 or less that can be solved in less than 4 minutes on standard hardware) by discarding the sensing configurations furthest away from the hotspot. Finally, the ERQ of the local solutions is retained in the vector $\mathbb{G}$.

C. Fusing the Local Solutions

In the simple case, in which hotspots are sufficiently far apart, we can obtain the global solution by solving the TSP to connect all the sensing configurations to form a tour. If this is not the case and the hotspots are close to each other (closer than two times the sensing range), there is the possibility that a configuration in the first local solution is very similar to another configuration from a second local solution. In this case, we eliminate redundant sensing configurations in a fusion step.

Nearby configurations are possibly redundant if they allow to perceive the considered hotspots from the same direction, which we define as an angular difference smaller then 15° of the configurations from the point of view of the hotspot.

All pairs of possibly redundant configurations are sorted by distance between the configurations, and another optimization problem, formulated in Eq. 7, is solved iteratively. The objective function in Eq. 7a minimizes the number of selected configurations and the constraint in Eq. 7b ensures that the overall loss of expected reconstruction quality of the fused solution compared to the local solutions is not bigger than δ.

In each iteration, two possibly redundant sensing configurations are substituted by a single fused configuration. Candidate positions C for the fused configuration are placed around both original configurations (within a radius of 1.5 times the sensing range) and evaluated. Eq. 8 has exactly the same structure as the optimization problem defined in Eq. 5. The ERQ of the hotspots in Z for each candidate configuration is computed by placing the remaining configurations in the sensing geometry, where H is the matrix of ERQ values for the cross angles.

If the number of selected configurations is less than or equal to one, the redundant configurations are fused and the list of the pairs is updated for the next iteration.

$$\underset{C}{\text{minimize}} \quad |C| \tag{7a}$$

subject to

$$ZC \succeq \mathfrak{g} - \delta \tag{7b}$$

$$C \in \{0,1\} \tag{7c}$$

$$Z = \alpha H + (1-\alpha)(\beta(\overline{\mathbf{1}'V}) + (1-\beta)(1-\overline{D})) \tag{8}$$

where $\mathfrak{g} \in \mathbb{G}$ is the local solution's ERQ.

With the fused list of configurations, the TSP connecting all the chosen sensing positions is solved. The resulting plan is then executed by the robot and the measurements are used to build a gas distribution map using a tomographic reconstruction algorithm in [11]. The overall procedure can be repeated in order to update the gas distribution map continuously.

IV. Experimental Evaluation

A. The Template Matching

To compare our algorithm with a straightforward and computationally less expensive method, template matching is used to place the configurations around each hotspot. Template matching places three fixed configurations with pair-wise cross angles of 60° and 120° based on the results of Sec. II. The position of the configuration is decided by casting a ray from the hotspot up to a distance equal to half the sensing range with the sensor always pointing towards the hotspot. If any of the three configurations can not be placed due to obstacles, the template is rotated iteratively with an increment of 1° clockwise and counter clockwise, until a valid placement is found or a full rotation is completed.

B. Solution Quality Evaluation

We evaluated the proposed ×vt-SPP algorithm in two different scenarios, namely the 120 m × 136 m Freiburg outdoor map[2], and the Örebro University (ORU) dataset as described in [2]. The ORU dataset contains measurements from indoor (61.5 m × 20 m) and outdoor (40.5 m × 16.5 m) locations where gas leaks were emulated using a set of transparent flasks filled with natural gas[3]. Details about the experiments can be found in [2].

In both cases, we compared the solution quality with the template matching algorithm. For the Freiburg outdoor map, 24 artificial hotspots were randomly placed and ×vt-SPP was used to generate a solution composed of 60 configurations with 645.50 m total traveling distance. Template matching on the other hand, produced a solution of 72 configurations and 714.25 m traveling distance.

The results for 10 different indoor and 5 different outdoor experiment runs from the ORU dataset are summarized in Table I. On average, the template matching results require 23% more sensing configurations, compared with ×vt-SPP. Similarly, the travel distance is 11% longer, compared with the measurement tours computed with ×vt-SPP.

TABLE I
Comparison between ×vt-SPP and template matching

Trials	Selected Conf.		Traveling Distance (m)	
	×vt-SPP	TM	×vt-SPP	TM
ORU Indoor 01	20	27	122.00	127.50
02	17	18	111.25	119.00
03	22	27	155.00	164.50
04	23	35	131.25	165.50
05	22	24	172.00	188.75
06	17	18	128.50	138.50
07	14	23	120.25	153.25
08	18	18	134.50	146.75
09	21	24	136.50	152.00
10	29	35	154.25	174.75
ORU Outdoor 01	24	33	139.50	164.00
02	20	24	129.50	134.25
03	20	24	174.00	192.00
04	19	24	105.75	98.00
05	17	18	114.75	111.50
Freiburg Outdoor	60	72	645.50	714.25

C. Real World Experiments

To evaluate the performance of ×vt-SPP in a real world gas distribution mapping problem, we conducted an experiment with the solution of our algorithm, template matching, and the strategy of a human expert[4] who is experienced in building gas distribution maps and conducted several experiments. The experiment was carried out in an indoor environment (Fig. 7(a)). Similarly to the ORU dataset, 12 transparent flasks filled with natural gas (90% methane) were placed at random locations.

All the experiments were performed using a Husky A200 called Gasbot (Fig. 2(a)). The robot is equipped with a Sewerin RMLD (TDLAS) methane sensor mounted on a pan-tilt unit to adjust the sensing range and field of view. A 3D range sensor (Velodyne HDL-32E) is used for mapping and localization. Mapping is carried out with the NDT-Fusion algorithm [12], while NDT-MCL [13] is used for the localization.

First, an exploration plan for gas detection was generated using the $conv$-SPP algorithm in [2]. Then, a coarse gas distribution map was generated [11] using the integral concentration measurements from the dataset (Fig. 7(b)). This coarse gas distribution map, with the identified hotspots, was used as an input for the template matching approach, for the human expert, and for ×vt-SPP. The solution with template matching comprised 27 configurations and a traveling distance of 168.75 m (Fig. 7(c)), the expert's strategy was 16 configurations with a 124.5 m traveling distance (Fig. 7(d)), and the solution from ×vt-SPP was 22 configurations and 154.00 m traveling distance (Fig. 7(e)). The corresponding gas distribution maps are shown in Fig. 8. Although, ×vt-SPP generated a higher number of configurations than the solution from the human expert, the quality of the map reconstruction with ×vt-SPP is comparatively higher as can be seen in Fig. 8. Notice the map generated from ×vt-SPP predicts high concentrations near the actual location of the gas flasks while for the human expert and template matching high concentrations tend to be spread over the map.

V. Conclusions

This paper addresses the problem of sensor planning for robot assisted gas tomography (RAGT). As the first step, we investigated sensing geometries and identified which combinations of sensing poses provide the highest reconstruction quality. We found that best results are obtained with a sensing geometry of 3 configurations with pair-wise 60° or 120° cross angles. We then included a preference for such local configurations in an optimization framework that selects the sensing configurations.

Finding the optimal solution of the problem is not feasible due to the complexity of the search space and the general uncertainty of the reconstruction quality estimation. We thus

[2]This is a publicly available map of the University of Freiburg campus, available at `https://www.openslam.org/gmapping.html`

[3]Due to safety regulations, we can not release methane in indoor environment.

[4]Dr. Victor Hernandez Bennetts, main author in [10], where RAGT was first introduced.

(a) Environment for the experiment

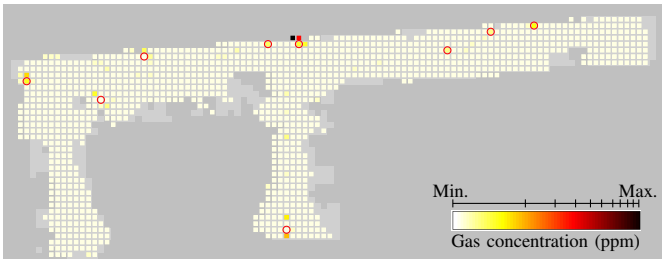

(b) Coarse gas distribution map

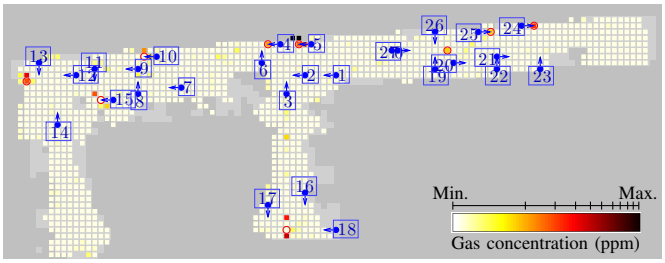

(c) Template matching solution

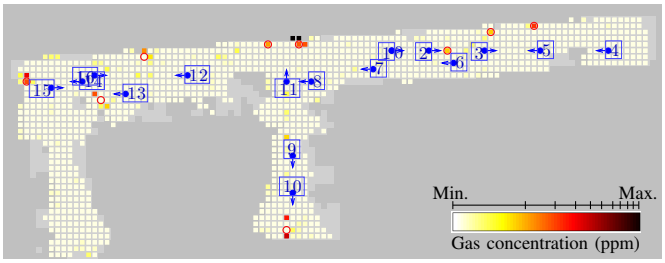

(d) Strategy of a human expert

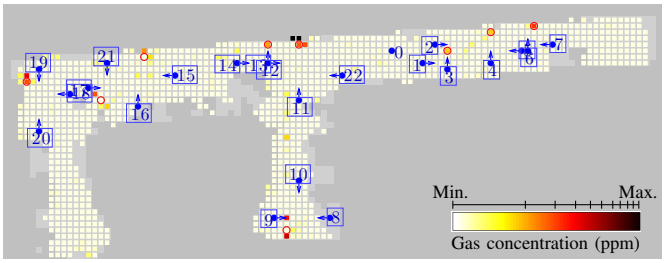

(e) $\times vt$-SPP solution

Fig. 7. Occupancy grid map of the environment for the experiment (a). The gas sources are indicated with red dots. Coarse gas distribution map built based on the data acquired in the gas detection step (b). For better visualization, the gas concentrations are shown with a nonlinear scale. All detected potential hotspots are marked with red circles. The sensor placement solutions for the tomographic reconstruction using the three strategies are shown in (c), (d), and (e). The selected configurations are indicated with blue dots (for the position) and arrows (for the orientation). The numbers indicate the execution sequence with 0 for the start position.

proposed a decoupled approach, the $\times vt$-SPP algorithm. It first generates sensing geometries for the hotspots individually and then combines these local solutions, fusing redundant sensing configurations. We find that $\times vt$-SPP generates better quality solutions than simplified, straightforward approaches (e.g. template matching). It requires a reasonable computation time in the order of a few minutes only – depending on the environment size, the number of high concentration regions (hotspots) and their location.

The approach was evaluated against a template matching method and a strategy suggested by a human expert. We first evaluated the solution quality in simulation experiments and found that $\times vt$-SPP generates sensing geometries with a fewer configurations and a shorter travel distance, compared with template matching.

With respect to the experiment in a real world environment, we observed that, while the solution of template matching uses more configurations and the solution proposed by the expert suggested fewer configurations, the solution computed with $\times vt$-SPP leads to maps of higher quality, with high concentrations estimated closer to the actual gas sources.

The behavior of the algorithm is dependent on the parameters α, β, δ and we will investigate in future work how to select those parameters. We will also further investigate the function used to estimate the expected reconstruction quality (ERQ). So far we assume that the environment does not introduce constraints on the cross angles and we want to also consider cases where pairwise 60° or 120° cross angles are not possible due to obstacles.

Furthermore, we will carry out a quantitative evaluation of the peak location error in the produced gas distribution maps. This is possible since we know the exact location of the gas sources (methane enclosed in bottles). Ground truth in a scenario with freely evaporating gas sources is, however, hard to obtain and typically not available in real-world experiments. This is a fundamental problem in mobile robotic olfaction. We therefore also plan to evaluate the proposed $\times vt$-SPP approach in complex simulated environments using a gas dispersion simulation [14].

References

[1] M. A. Arain, M. Trincavelli, M. Cirillo, E. Schaffernicht, and A. J. Lilienthal, "Global Coverage Measurement Planning Strategies for Mobile Robots Equipped with a Remote Gas Sensor," *Sensors*, vol. 15, no. 3, pp. 6845–6871, 2015.

[2] M. A. Arain, M. Cirillo, V. Hernandez Bennetts, E. Schaffernicht, M. Trincavelli, and A. J. Lilienthal, "Efficient Measurement Planning for Remote Gas Sensing with Mobile Robots," in *IEEE International Conference on Robotics and Automation (ICRA)*. Seattle, WA, USA: IEEE, 2015, pp. 3428–3434.

[3] V. Hernandez Bennetts, E. Schaffernicht, T. Stoyanov, A. J. Lilienthal, and M. Trincavelli, "Robot Assisted Gas Tomography - Localizing Methane Leaks in Outdoor Environments," in *IEEE International Conference on Robotics & Automation (ICRA)*. Hong Kong, China: IEEE, 2014, pp. 6362–6367.

[4] R. Byer and L. Shepp, "Two-dimensional remote air- pollution monitoring via tomography," *Optical Letters*, vol. 4, no. 3, pp. 75–77, 1979.

[5] A. Hartl, B. C. Song, and I. Pundt, "2-D reconstruction of atmospheric concentration peaks from horizontal long path DOAS tomographic measurements: parametrisation and geometry within a

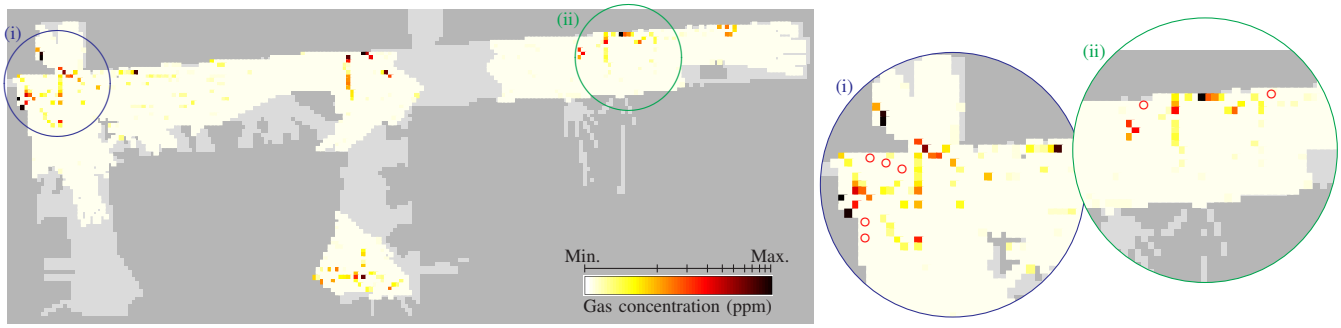

(a) Template matching

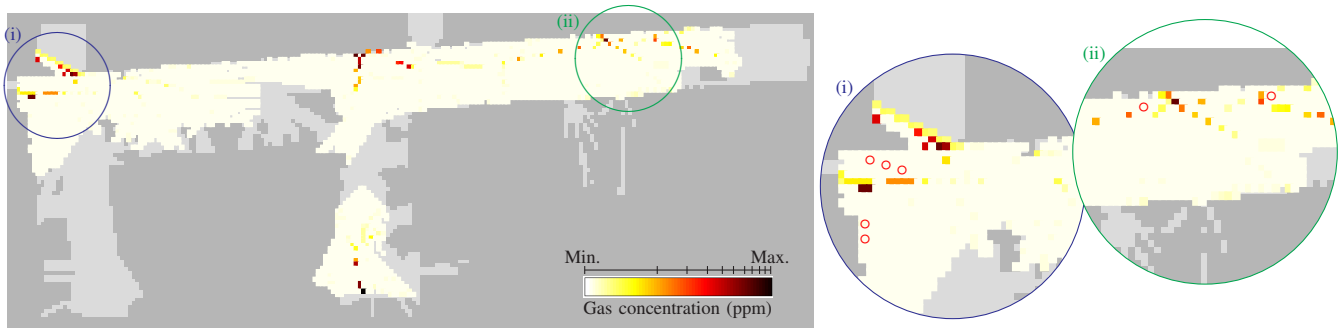

(b) Strategy of a human expert

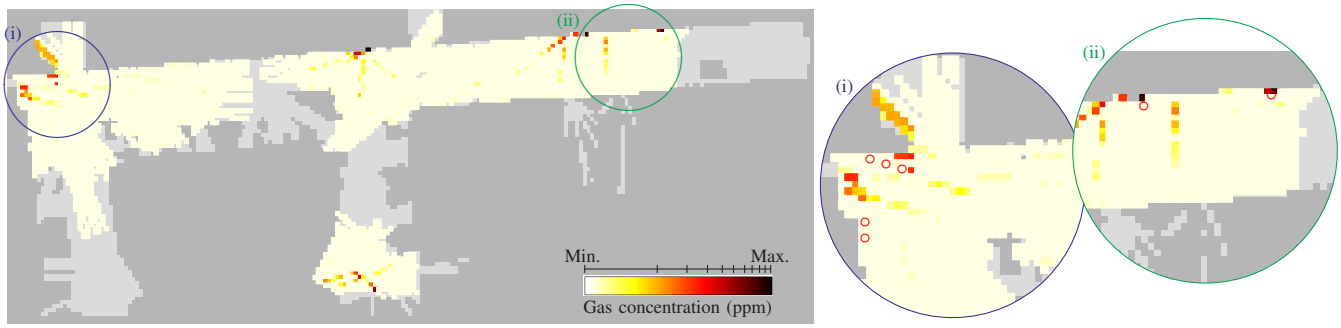

(c) $\times vt$-SPP algorithm

Fig. 8. The resulting gas distributions maps from the three strategies are shown with the same color code as in Fig. 7. Magnified sections of interesting areas are shown on the right, where the position of gas sources is marked with small red circles. For both areas of interest, the resulting reconstruction using the $\times vt$-SPP generated measurement positions highlights the gas sources better than the gas maps built using the measurements based on the human expert's strategy or the template matching.

discrete approach," *Atmospheric Chemistry and Physics*, vol. 6, no. 3, pp. 847–861, Mar. 2006.

[6] L. A. Todd and R. Bhattacharyya, "Tomographic reconstruction of air pollutants: evaluation of measurement geometries," *Applied Optics*, vol. 36, no. 30, pp. 7678–7688, 1997.

[7] B. R. Cosofret, D. Konno, A. Faghfouri, H. S. Kindle, C. M. Gittins, M. L. Finson, T. E. Janov, M. J. Levreault, R. K. Miyashiro, and W. J. Marinelli, "Imaging Sensor Constellation for Tomographic Chemical Cloud Mapping." *Applied optics*, vol. 48, no. 10, pp. 1837–1852, 2009.

[8] W. Verkruysse and L. A. Todd, "Improved method grid translation for mapping environmental pollutants using a two-dimensional CAT scanning system," *Atmospheric Environment*, vol. 38, no. 12, pp. 1801–1809, Apr. 2004.

[9] N. Atanasov, J. L. Ny, K. Daniilidis, and G. J. Pappas, "Information Acquisition with Sensing Robots: Algorithms and Error Bounds," in *IEEE International Conference on Robotics & Automation (ICRA)*. Hong Kong, China: IEEE, 2014, pp. 6447–6454.

[10] V. Hernandez Bennetts, A. J. Lilienthal, A. A. Khaliq, V. P. Sese, and M. Trincavelli, "Towards Real-World Gas Distribution Mapping and Leak Localization Using a Mobile Robot with 3D and Remote Gas Sensing Capabilities," in *IEEE International Conference on Robotics and Automation (ICRA)*. Karlsruhe, Germany: IEEE, 2013, pp. 2335–2340.

[11] M. Trincavelli, V. H. Bennetts, and A. J. Lilienthal, "A Least Squares approach for learning gas distribution maps from a set of integral gas concentration measurements obtained with a TDLAS sensor," in *IEEE Sensors*. Taipei, Taiwan: IEEE, 2012, pp. 1–4.

[12] T. Stoyanov, J. Saarinen, H. Andreasson, and A. J. Lilienthal, "Normal Distributions Transform Occupancy Map Fusion: Simultaneous Mapping and Tracking in Large Scale Dynamic Environments," in *EEE/RSJ International Conference on Intelligent Robots and Systems (IROS)*, Tokyo Big Sight, Japan, 2013, pp. 4702–4708.

[13] J. Saarinen, H. Andreasson, T. Stoyanov, and A. J. Lilienthal, "Normal Distributions Transform Monte-Carlo Localization (NDT-MCL)," in *EEE/RSJ International Conference on Intelligent Robots and Systems (IROS)*, Tokyo Big Sight, Japan, 2013, pp. 382–389.

[14] V. Hernandez Bennetts, A. J. Lilienthal, E. Schaffernicht, S. Ferrari, and J. Albertson, "Integrated Simulation of Gas Dispersion and Mobile Sensing Systems," in *RSS Workshop on Realistic, Rapid and Repeatable Robot Simulation (R4SIM)*, 2015.